

## The Bering Slope Current System Revisited\*

GREGORY C. JOHNSON AND PHYLLIS J. STABENO

*NOAA/Pacific Marine Environmental Laboratory, Seattle, Washington*

STEPHEN C. RISER

*School of Oceanography, University of Washington, Seattle, Washington*

(Manuscript received 28 January 2003, in final form 7 August 2003)

### ABSTRACT

Mean circulation and water properties within the Aleutian Basin of the Bering Sea are investigated using hydrographic and subsurface pressure displacement data from a regional array of 14 profiling CTD floats. After 10 days drifting at 1000 dbar, each float measures temperature and salinity profiles as it rises to the surface and then transmits these data via satellites, which also make several fixes of the float surface positions before it sinks again. Every fourth cycle, the floats sink from 1000 dbar to a 2000-dbar target just prior to ascent to measure deeper profiles. The 1000-dbar displacements estimated from the float surface position fixes reveal a coherent few-centimeters-per-second northwestward flow along the northeastern boundary, the deep signature of the Bering Slope Current. Middepth water property distributions are consistent with cyclonic advection of warm water from the south around the basin, eastward in the Aleutian North Slope Current, and then northwestward in the Bering Slope Current. Geostrophic transport estimates relative to 1000 dbar also show cyclonic motion, although with significant noise, likely owing to the influence of mesoscale eddies. The mean along-slope geostrophic transport of the Bering Slope Current is determined between 0 and 1900 dbar relative to 1000 dbar and then combined with mean along-slope velocities at 1000 dbar. The result is an absolute geostrophic transport estimate with 95% confidence intervals for the along-slope current offshore of the 1000-m isobath and between 0 and 1900 dbar of  $5.8 (\pm 1.7) \times 10^6 \text{ m}^3 \text{ s}^{-1}$ .

### 1. Introduction

The Bering Sea, located between Siberia and Alaska, is bounded to the south by the arc of the Komandorskiye and Aleutian Islands and to the north by Siberia, with a narrow connection to the Arctic Ocean through the Bering Strait (Fig. 1). The northeast portion of the sea is a wide and shallow continental shelf. The deep portion of the sea is divided into three connected deep basins, the largest of which is the Aleutian Basin. The smaller Bowers Basin is partly enclosed by the Bowers Ridge, and the equally small Kamchatka Basin is partly enclosed by the Shirshov Ridge. While the Bering Strait to the north is shallow, there are numerous passes and straits within the island arc to the south, with the deepest three being Kamchatka Strait ( $164^\circ\text{E}$ ,  $\sim 3600\text{-m}$  sill depth), Near Strait ( $170^\circ\text{E}$ ,  $\sim 2000\text{ m}$ ), and Amchitka Strait ( $180^\circ$ ,  $\sim 1000\text{ m}$ ).

The surface circulation of the Bering Sea has been estimated using satellite-tracked drifters (Stabeno and Reed 1994), and can roughly be described as a cyclonic gyre (Stabeno et al. 1999). Currents within the region include an eastward flow along the southern boundary of the deep Bering Sea, fed by northward flow through the island arc passes and straits mentioned above (Reed and Stabeno 1994), named the Aleutian North Slope Current; a northwestward flow along the northeast continental slope of the Aleutian Basin, the Bering Slope Current (Kinder et al. 1975); and a southward flow offshore of Kamchatka that exits the Bering sea through the Kamchatka Strait, the Kamchatka Current (Verkhunov and Tkachenko 1992). However, apart from a few isolated current-meter records (Schumacher and Reed 1992; Cokelet and Stabeno 1997), there are very few direct measurements of the subsurface flow in the deep Bering Sea.

Much of the knowledge of the subsurface circulation of the Bering Sea has come through application of the geostrophic relation to data from hydrographic surveys to estimate the flow field relative to a reference level of no motion, or occasionally, one of known motion. In the Bering Sea, a level of no motion is often assumed to hold somewhere between 500 and 1500 m (Kinder

\* Pacific Marine Environmental Laboratory Contribution Number 2540.

*Corresponding author address:* Dr. Gregory C. Johnson, NOAA/Pacific Marine Environmental Laboratory, 7600 Sand Point Way N.E., Bldg. 3, Seattle, WA 98115-6349.  
E-mail: gregory.c.johnson@noaa.gov

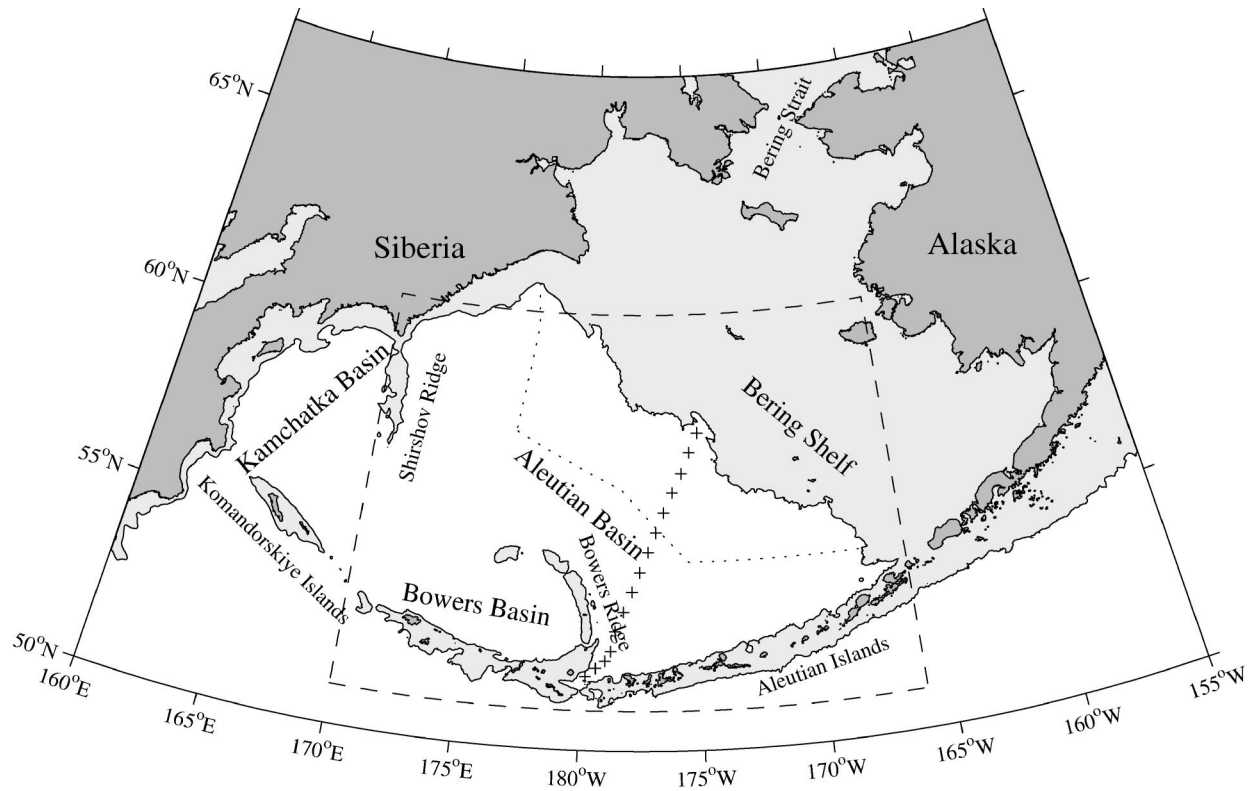


FIG. 1. Bering Sea region with place names. Depths shallower than 1000 m are lightly shaded, and land is heavily shaded using version-8.2 bathymetry of Smith and Sandwell (1997). The dashed line indicates the float array region, and the Bering Slope Current study region is located northeast of the dotted line. Locations (+) of WOCE section P14N CTD stations used for float CTD salinity evaluation and calibration are indicated.

et al. 1975; Reed 1995b). This assumption is often necessitated by hydrographic station data that stop at mid-depth. The assumption is also usually applied with the acknowledgment that the level of no motion is in reality likely to be a level of weak motion. Since the absolute velocity field is only known in a few isolated locations at depth (and the surface velocity field measured by Lagrangian drifters is not expected to be in close geostrophic balance because of near-surface Ekman dynamics), often no better alternative has been available. Water property distributions from hydrographic surveys, such as the relative strength of the subsurface temperature minimum (Kinder et al. 1975; Sayles et al. 1979), are sometimes used to corroborate geostrophic calculations.

Middepth levels of no motion are prevalent in the Bering Sea literature. The few full-depth hydrographic surveys there (e.g., Roden 1995) show that geostrophic shear, while it weakens with increasing depth, often persists with a single sign to the abyssal seafloor. Geostrophic velocities referenced to directly measured currents from a shipboard acoustic Doppler current profiler (ADCP) have amplitudes of a few centimeters per second even at the abyssal sea floor (Cokelet et al. 1996). Thus velocities apparently reach much deeper than 500 or even 1500 m in the Bering Sea. While application of a middepth level of no motion apparently does not

introduce much error in near-surface velocity estimates within the boundary currents (Reed 1995b), it can introduce error in the boundary current transport estimates because even weak deep velocities result in large transports when integrated over current cross sections (Cokelet et al. 1996).

Other potentially confounding influences on current transport estimates are the energetic eddies that are so prevalent in the Bering Sea. These eddies have been studied using various combinations of hydrographic, drifter, satellite sea-surface temperature, current meter, and satellite sea-surface height data (Kinder et al. 1980; Paluszkiwicz and Niebauer 1984; Schumacher and Staben 1994; Okkonen 2001; Mizobata et al. 2002). These eddies reach length scales around 100 km and time scales of a few months. Most synoptic hydrographic surveys contain such eddies, whether they resolve them or not, and eddies at the edge of a hydrographic survey that are not sampled completely can badly bias transport estimates. Combining velocity data from drifters (Kinder et al. 1980) and shipboard ADCPs (Cokelet et al. 1996) with hydrographic data suggests that these eddies have a significant expression (several centimeters per second) at middepth, and even at the abyssal seafloor.

Last, there is a strong seasonal cycle in wind forcing over the deep Bering Sea (Bond et al. 1994), with Ek-

man suction sufficient to drive a cyclonic gyre in topographic Sverdrup balance in the Bering Sea with a volume transport as large as 15 Sv ( $1 \text{ Sv} \equiv 10^6 \text{ m}^3 \text{ s}^{-1}$ ) in winter and as small as zero in the summer. Numerical model results suggest a strong seasonal variation in gyre strength (Overland et al. 1994). Geostrophic transports within the Kamchatka Current estimated above a 1500-dbar level of no motion were certainly stronger in a spring hydrographic survey than those estimated 6 months later in a fall survey (Verkhunov and Tkachenko 1992). This change is consistent with the hypothesized seasonal cycle, but there are probably not enough hydrographic data to distinguish seasonal from interannual transport variations (Stabeno and Reed 1992).

An array of 22 profiling floats has been deployed in the Bering Sea and subpolar North Pacific south of the Aleutian Islands to provide a large-scale context for study of interannual variability in ocean water properties and currents within the Bering Sea and around the Aleutian Islands. Here we use hydrographic and 1000-dbar park pressure displacement data from the 14 profiling floats deployed in the Aleutian Basin of the Bering Sea to investigate the water properties and absolute circulation there. This study is limited to the eastern side of the basin, focusing on the Bering Slope Current. Float displacements at their 1000-dbar park pressure are used to make estimates of the flow field at that pressure (Davis 1998). Vertical profiles of temperature and salinity from the floats are used to analyze water-property distributions. These same profiles are used for geostrophic calculations relative to 1000 dbar, which are then combined with the 1000-dbar velocity estimates to determine an absolute along-slope transport for the Bering Slope Current offshore of the 1000-m isobath. The data are distributed over seasons and the mesoscale eddy field, so the errors from these sources of noise in the determination of a mean circulation can be estimated.

## 2. Data

Fourteen profiling CTD (conductivity–temperature–depth) floats were deployed in the Aleutian Basin of the Bering Sea over a 1-yr period (five in May–June 2001, five in July–August 2001, and four in May 2002). The floats were built at the University of Washington from components purchased from Webb Research Corp. Each float is equipped with a SBE-41 CTD from SeaBird Electronics, Inc. The floats are programmed to drift freely at their 1000-dbar park pressure for 10 days, then rise to the surface in under 3.5 h, collecting CTD data at predetermined pressures during their ascent. They then remain on the ocean surface for about 11 h, where they transmit data and their positions are determined by satellite (Service Argos, Inc.). Every fourth cycle, the floats sink from their park pressure to a target of 2000 dbar just before rising to the surface, collecting data from that pressure up and remaining on the surface for about 7 h. Nominally 70 measurements are made during

the 2000-dbar profiles, and 60 during the 1000-dbar profiles. Data are taken at widely spaced pressure intervals at depth, and more closely spaced intervals approaching the surface, to resolve upper ocean features. Samples are taken at 100-dbar intervals from 2000 to 600 dbar, 50-dbar intervals to 400 dbar, 20-dbar intervals to 300 dbar, 10-dbar intervals to 150 dbar, 5-dbar intervals to 60 dbar, and 4-dbar intervals to 8 dbar (the shallowest sampling pressure). Over about 26 months, 775 profiles from 14 floats have been collected in the Bering Sea.

The floats are estimated to have sufficient energy to complete over 200 cycles each, well over 5 years. However, two of the floats deployed in the Bering Sea have already stopped reporting after running aground in shallow areas with vigorous tidal flows. Some of the remaining floats in the basin are susceptible to a manufacturing defect, which may significantly shorten their lifetimes. A realistic mean lifetime for the remaining floats subject to these and other hazards might be 4 years. In this event, the floats should report roughly 900 more profiles. Thus analyses like those below, but made in the future after all the floats have stopped reporting, might have uncertainties about two-thirds of the present values.

The CTD manufacturer claims initial accuracies of 0.005 for salinity,  $0.002^\circ\text{C}$  for temperature, and 2.4 dbar for pressure. The latter two measurements are likely to remain accurate for a long time, but shipboard CTD experience suggests that the salinity calibration may drift with time. However, salinity measurements from the floats are remarkably stable and accurate with respect to the deep potential temperature–salinity ( $\theta$ – $S$ ) relation. The 15 deep stations from the World Ocean Circulation Experiment (WOCE) section P14N taken across the Aleutian Basin (Fig. 1) in 1993 (Roden 1995) have a mean and standard deviation of  $S = 34.531 (\pm 0.002)$  at  $\theta = 2^\circ\text{C}$  (near 1700 dbar). Each of the floats have similar standard deviations (between 0.0004 and 0.004) for this quantity, and no obvious salinity calibration drifts over their lifetimes to date. Such stable  $S$  measurements appear typical of these instruments over even longer deployments. The differences between the WOCE section mean value and the individual float mean values have a mean and standard deviation of 0.004 ( $\pm 0.005$ ). Eight of the floats overlap with the WOCE salinity measurements within standard deviations, while the rest report fresher values than WOCE. The largest such discrepancy is 0.016, a difference about thrice the accuracy claimed by the manufacturer. The temporal stability of the salinity data from individual floats and the spatial uniformity of salinity at  $\theta = 2^\circ\text{C}$  in the Aleutian Basin imply that such offsets among the float data almost certainly result from salinity calibration errors in the individual floats. Hence, each float has been adjusted so that its mean salinity at  $\theta = 2^\circ\text{C}$  matches that for the P14N data, a crude version of a correction to the climatological  $\theta$ – $S$  relation (Wong et al. 2003) that

probably results in salinity data accurate to 0.005 or better in this case.

Float displacements at the 1000-dbar park pressure are estimated from the differences in position between the last position fix before a float sinks and the first position fix after it rises again divided by the time elapsed between these fixes, about 10.25 days. To date 775 displacements have been measured in the Bering Sea, which is over 21 float-years of data. The mean and standard deviation of the displacement speeds are  $0.039 (\pm 0.024) \text{ m s}^{-1}$ . Two possible sources of error arise from this simple method of velocity estimation. The first error source is unmeasured surface drift. The second source is the drift of the float as it passes through subsurface currents while rising and sinking. In each case the errors can be estimated by the ratio of the unmeasured drift in question to the 1000-dbar displacement. These two errors are estimated below to be on the order of 5% each. Since they are likely to be correlated, they probably sum to around 10%.

Floats stay on the surface for 10 h on average, and the mean time between the first and last position fixes from each surfacing is 8 h. Hence 2 h (or 20%) of the float surface drift is typically unaccounted for and erroneously ascribed to the park pressure displacements. The float surface drift speeds,  $0.22 (\pm 0.14) \text{ m s}^{-1}$ , are estimated crudely from the distance from the first to the last position fix for each float surfacing divided by the time elapsed between those fixes. The product of the mean float surface drift speeds and the two unmeasured hours gives an estimate of the unmeasured surface displacement. This estimate is less than 5% of the mean displacements from the last position fixes before each float sinks and the first position fixes after it rises. This ratio is the estimate of the first error source.

The float buoyancy is controlled to keep a minimum ascent rate of  $0.08 \text{ m s}^{-1}$ , and so the float takes around 3.5 h to rise from 1000 dbar to the surface. Upon initiation of descent, the float buoyancy is rapidly targeted to the park pressure, so the float sinks rapidly near the surface, and slows with increasing pressure, reaching one-half of its park pressure in under 2 h (Davis et al. 1992). For the error estimate of the effect of unmeasured velocities during float rise and descent, the transition from near-surface velocities to park velocities is assumed to follow the structure of the mean vertical density structure, and so upper-ocean velocities are surface intensified above the pycnocline. Of course, float surface velocities are not strictly representative of upper-ocean velocities, both because surface velocities may include a large Ekman velocity and because the floats do not follow water parcels well while at the surface (Davis et al. 1992). Despite these problems, the mean surface and park displacement speeds are combined with ascent rates, descent rates, and the mean vertical density profile to obtain a rough estimate that subsurface currents introduce an additional error of 5% in the park displacement velocities.

These floats do occasionally run aground, potentially introducing significant biases into their displacement data. If either the last position fix before descent or the first position fix after surfacing is over water shallower than 1000 m, according to a high-resolution bathymetry (Smith and Sandwell 1997, version 8.2), the park depth datum is deemed subject to biases from float grounding and is omitted from any calculations. This screening eliminates 26 out of 775 float displacements.

### 3. Middepth velocities

The largest float displacements (highest speeds) occur when the floats are describing roughly circular motions (both cyclonic and anticyclonic) with radii sometimes approaching 80 km (Fig. 2). The radii are much larger than the local 17-km first baroclinic radius of deformation for the Bering Sea (Chelton et al. 1998), but typical of scales reported by regional eddy analyses mentioned above. The floats take around 60 days to make a single circuit, although not many stay in an eddy for more than a circuit or two. Speeds at the outer limits of these eddies can reach  $0.1 \text{ m s}^{-1}$  at 1000 dbar. Eddies of similar size have been observed in hydrographic data (Kinder et al. 1980), where surface velocities measured by drifters exceeded surface geostrophic velocities referenced to 1500 dbar in the eddies by around  $0.08 \text{ m s}^{-1}$ . These velocity differences were early indirect estimates of the eddy velocities at 1500 dbar and are very close to the faster 1000-dbar eddy velocities observed directly by the floats. Geostrophic velocities referenced to shipboard ADCP data also concur that eddy velocities are significant at 1000 dbar and suggest that their signature may extend to the bottom (Cokelet et al. 1996).

Lagrangian integral time and space scales are estimated from the park pressure meridional and zonal velocities for each float record. Since the floats spend some time at the surface, they are not truly Lagrangian at their park pressure. Nonetheless these quantities may allow quantification of the number of degrees of freedom in the 1000-dbar velocity data. For each float and each velocity component the autocovariances are integrated from zero time lag out to their first zero crossings to give an upper bound on these quantities (Poulain and Niiler 1989). Means and standard deviations of autocovariance zero crossings are  $45 (\pm 40)$  days for  $u$  and  $25 (\pm 15)$  days for  $v$ . Integral time scales are  $11 (\pm 6)$  days for  $u$  and  $9 (\pm 4)$  days for  $v$ . Standard deviations of  $u$  and  $v$  are around  $0.03 \text{ m s}^{-1}$  for the floats, which when multiplied by the corresponding integral time scales give zonal and meridional Lagrangian integral space scales of  $31 (\pm 17)$  km and  $25 (\pm 11)$  km, respectively. There is undoubtedly spatial variability of these scales, but it would be difficult to estimate with the data presently available. Overall, the array is sufficiently sparse that floats sample the same flow only rarely, and the sampling interval is on average very near the Lagrangian integral time scale. Therefore, the data

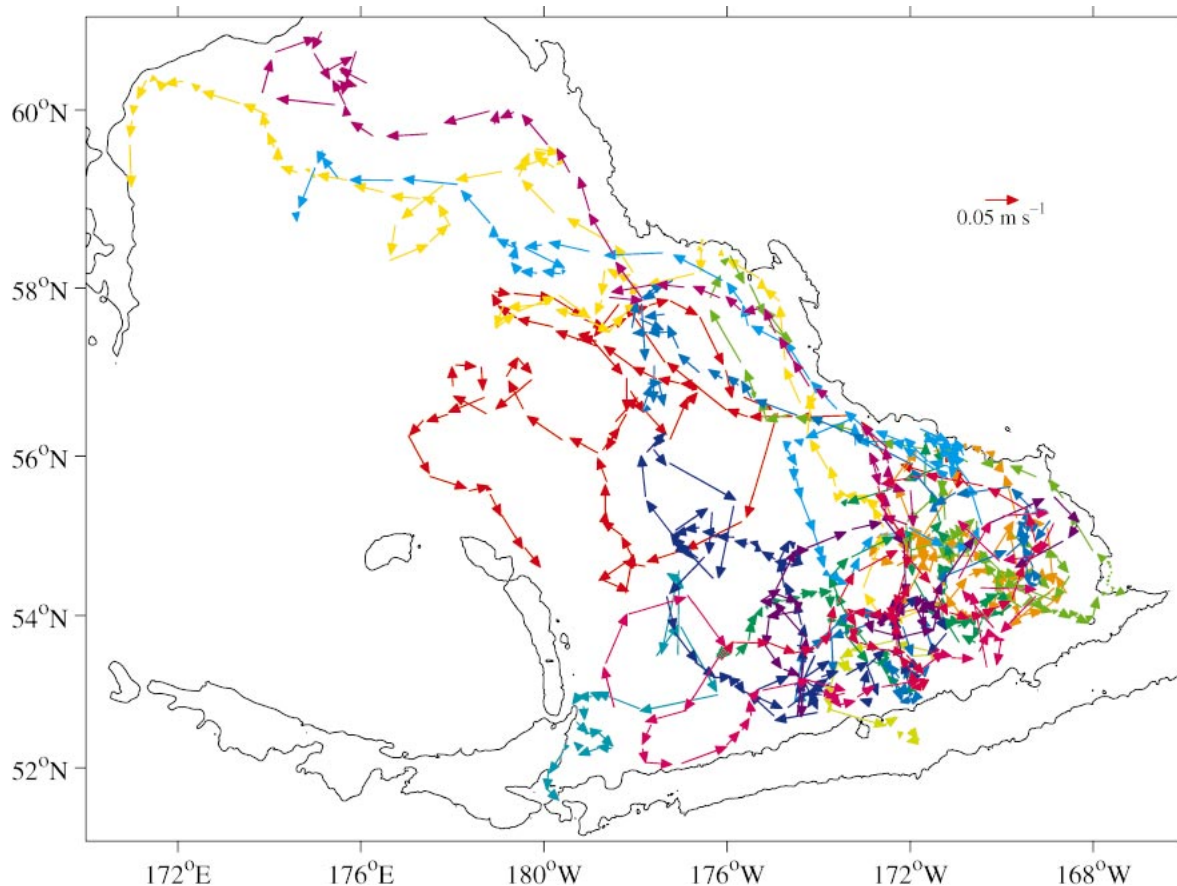


FIG. 2. All 10-day displacements at 1000 dbar (including grounded values) from the CTD profiling floats in the Bering Sea. A velocity scale is over the Bering Shelf. The 1000-m isobath (thin line) is displayed for reference. Each float is a different color.

suggest that on average each park pressure displacement is nearly statistically independent and contributes a degree of freedom for the purposes of error estimates.

The 1000-dbar velocity data are analyzed in  $0.5^\circ$  latitude by  $1^\circ$  longitude bins (roughly 55 km by 55 km at these latitudes) to produce a mean field with error estimates (Fig. 3). First float displacements from apparently grounded instruments are excluded. Then velocities are computed from displacements and each velocity is assigned a position that is the average of the last position fix before the float sinks and the first position fix after it rises again. The mean velocity in each bin is computed. Deviations from those means are used to compute a current ellipse (Emery and Thomson 1997). The current ellipses are scaled using the number of degrees of freedom in the bin and Student's  $t$  distribution to obtain a 95% confidence limit for the mean velocity vectors (Fig. 3). Only results from bins with three or more measurements are displayed, and those bins have a mean and standard deviation of  $7 (\pm 5)$  observations each. Mean velocities are generally less than  $0.05 \text{ m s}^{-1}$ , not well organized, and not significantly different from zero at 95% confidence limits (Fig. 3). With vigorous eddy signatures in much of the Bering Sea, even

at 1000 dbar, and the small sample size in many of the bins, it is not surprising that the mean there is difficult to determine.

The one exception to this lack of pattern is the group of more rapid and coherent northwestward velocities found offshore of the Bering Shelf, the 1000-dbar signature of the Bering Slope Current. This current is visible in the individual float displacements (Fig. 2) and in the general tendency for the mean velocities in the bins close to the 1000-m isobath to flow northwestward, paralleling it (Fig. 3). Many of the mean values in these bins are significantly different from zero at 95% confidence limits. Since geostrophic transport estimates of this current frequently assume a level of no motion near this pressure, accurate estimates of the observed along-slope velocity at this pressure are desirable to improve transport estimates. The Aleutian North Slope Current is not apparent in the float displacements, perhaps because it is centered over the 1000-m isobath and is narrower than the Bering Slope Current (Stabeno and Reed 2003, unpublished manuscript).

More detailed estimates of the along-slope velocity field at 1000 dbar associated with the Bering Slope Current are made. First, the closest range to the 1000-m

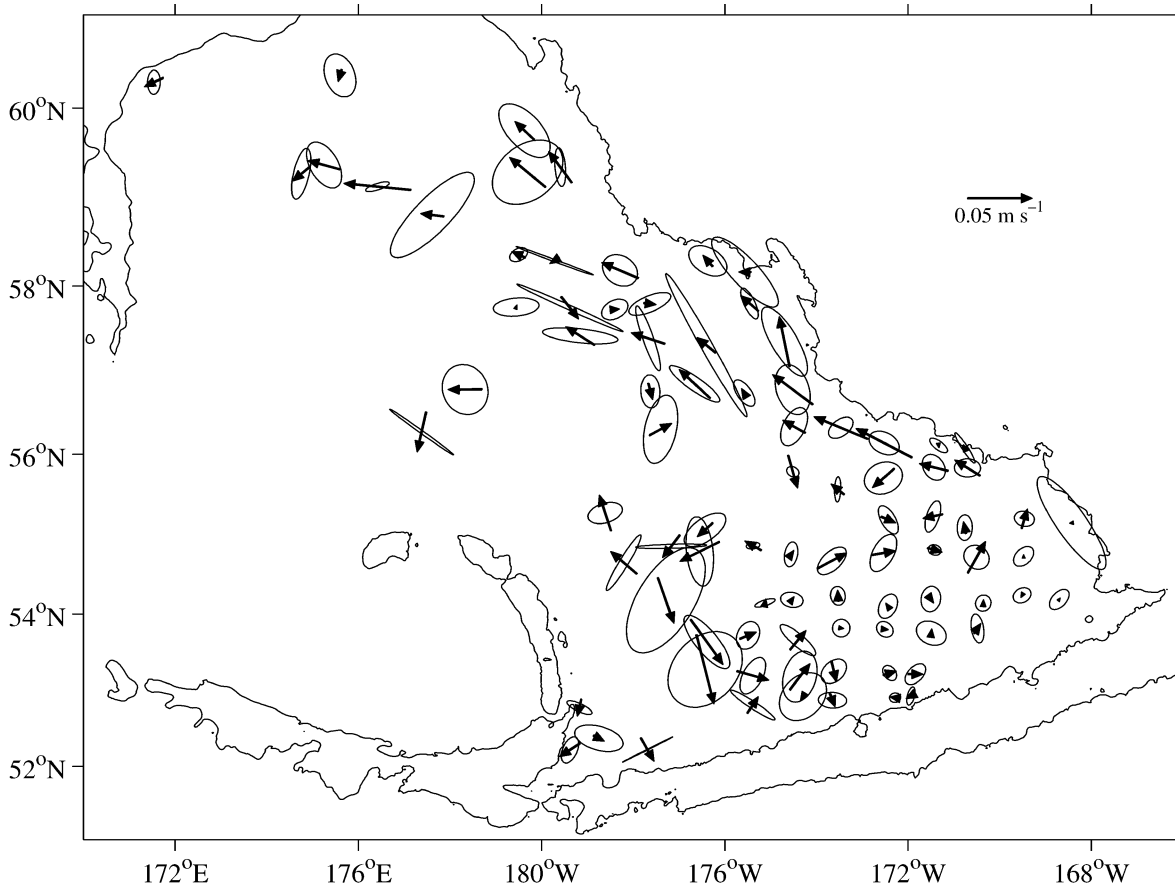


FIG. 3. Mean velocities and error ellipses at 1000 dbar constructed from analysis of individual float displacements (excluding grounded values) in  $0.5^\circ$  lat by  $1^\circ$  lon bins. Results from bins containing at least three measurements are shown, using 88% of the individual displacements. Arrows are centered on the mean position of the velocity measurements within the bins. Current error ellipses are scaled so that if the mean vector reaches outside the error ellipse, it is significant at 95% confidence limits. Details follow Fig. 2 except for a change in velocity scale.

isobath and the bearing associated with that range are found for last position fix before descent and the first position fix after surfacing associated with each float park displacement velocity. These two ranges and bearings are averaged for each velocity estimate. Only data within the region containing the current are included (southwest of the Bering Shelf within the Aleutian Basin, Fig. 1). There are 343 velocity estimates within the study region—over 9 float-years of data. The mean bearing to the 1000-m isobath for each velocity estimate is used to rotate the velocity data into along-slope and across-slope components of the flow. The along-slope velocities are then averaged according to the mean range from the 1000-m isobath for each velocity estimate in 20-km bins, containing between 24 and 43 points in each bin out to 160 km (Fig. 4), and fewer farther from the 1000-m isobath.

The signature of the Bering Slope Current is evident in the bins closest to the 1000-m isobath. Values in the bins 30 and 50 km from the 1000-m isobath (positive values signify flow in a cyclonic sense around the basin) are significantly different from zero within 95% con-

fidence limits, the uncertainties quoted, whereas the bins farther from the 1000-m isobath have values that are much closer to zero and are not statistically different from zero. Along-shore velocities reach as high as  $0.033 (\pm 0.012) \text{ m s}^{-1}$  at 30 km from the 1000-m isobath.

These 1000-dbar flows are used below as a level of known motion for geostrophic transport estimates made between the surface and 1900 dbar, relative to 1000 dbar, and offshore of the 1000-m isobath. While these flows are not large when compared with surface velocities (Stabeno and Reed 1994), even small flows integrated over the water column can amount to a significant transport. The contribution of these level of known motion velocities when applied depth independent over 1900 dbar and integrated offshore of the 1000-m isobath as a function of range out to 120-km distance amounts to  $3.0 (\pm 0.9) \text{ Sv}$  (Fig. 4). This value alone is over one-half of the previous 5-Sv transport estimate for the Bering Slope Current above a 1500-dbar level of no motion (Kinder et al. 1975). The 1900-dbar limit on the analysis is set by the maximum pressure sampled by the bulk of the deeper profiles. The median distance between the

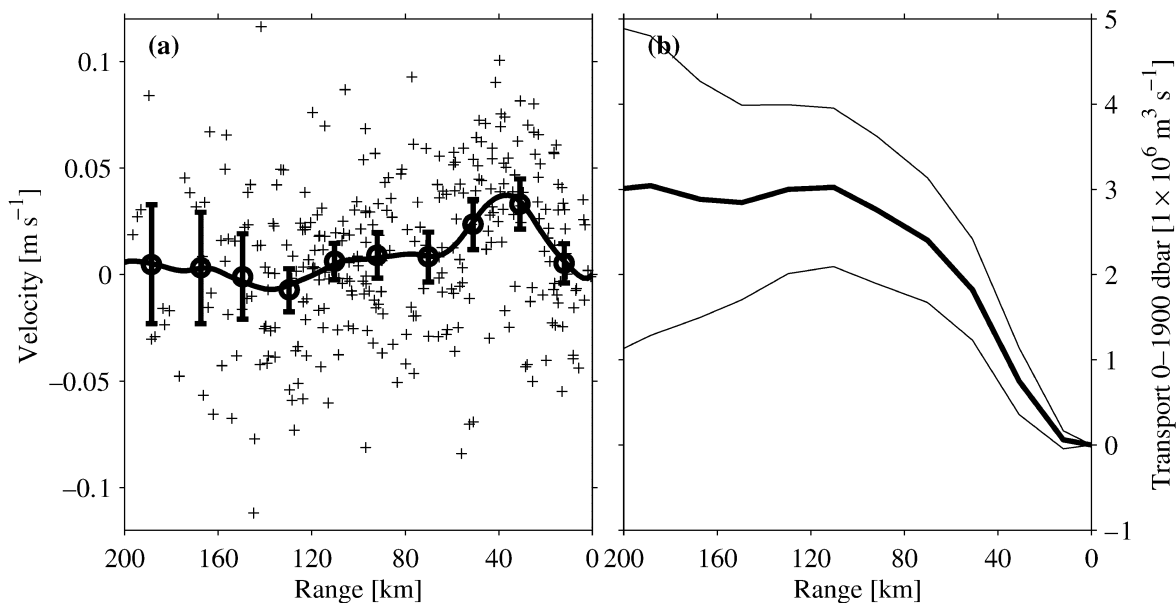


FIG. 4. (a) Along-slope velocities at 1000 dbar within the Bering Slope Current plotted against range from the 1000-m isobath with raw values (+), averages in a 20-km bins ( $\circ$ , with error bars showing 95% confidence intervals), and a smooth curve drawn using a loess filter with a 40-km half-power point (thick line). (b) Cumulative transport (thick line) resulting from application of the binned 1000-dbar velocities over 0–1900 dbar integrated as a function of range from the 1000-m isobath with 95% confidence intervals (thin lines). Range is plotted in reverse to associate northeast with the right-hand side.

1000- and 1900-m isobaths is only 8 km between  $55^\circ$  and  $60^\circ\text{N}$  off the Bering Shelf. Since there is very little alongshore flow at 1000 dbar within 10 km of the 1000-m isobath and the continental slope is so steep, the bathymetry offshore of the 1000-m isobath does not significantly affect this transport measurement. However, any flow inshore of the 1000-m isobath is neglected in this estimate.

#### 4. Water property distributions

The Bering Sea pycnocline is dominated by salinity stratification, with a stabilizing layer of fresh water overlying saltier water at depth (Fig. 5a; Roden 1995). In contrast, the  $\theta$  distribution includes a subsurface maximum within the permanent pycnocline (Fig. 5b: near 300 dbar) that originates from inflow of relatively warm Alaska Stream water into the Bering Sea through the passes in the southern island arc (Sayles et al. 1979; Reed 1995a), modified by strong mixing within the passes. Above that maximum is a  $\theta$  minimum (Fig. 5b, thick line near 200 dbar), evident below the seasonal thermocline in all but the most extreme winter conditions (Fig. 5b, thin line), when the minimum is renewed by surface cooling (Cokelet and Stabeno 1997; Miura et al. 2003). These water property features can be used to infer the circulation patterns (Kinder et al. 1975). The hydrographic data collected by the floats are analyzed here to examine temporal and spatial variations in these features.

The mean and median potential densities of the sub-

surface  $\theta$  minimum are both near  $\sigma_\theta = 26.60 \text{ kg m}^{-3}$ . This value is only slightly less than the maximum mixed layer values observed by the floats,  $\sigma_\theta > 26.60 \text{ kg m}^{-3}$  in winter 2001/02 and  $>26.64 \text{ kg m}^{-3}$  in 2002/03, as would be expected for a feature renewed by wintertime surface cooling. In both of these winters the surface mixed layer pressures sometimes exceed 200 dbar, near the pressure of the  $\theta$  minimum. There is spatial variability in the wintertime mixed layer distributions, with lighter and shallower winter mixed layers found toward the southeast.

While there is substantial scatter in  $\theta$  on  $\sigma_\theta = 26.60 \text{ kg m}^{-3}$ , partly due to spatial variations discussed below, the data do suggest a seasonal cycle when plotted against time (Fig. 6). These data are analyzed by fitting annual and semiannual harmonics to all the data used to define a regional seasonal cycle and then removing that seasonal cycle before mapping the mean spatially. This method assumes that the array has fairly even spatial and temporal coverage and that the magnitude of the seasonal cycle is nearly spatially uniform. It is likely that neither of these assumptions is perfectly satisfied, but the method does allow for spatial variations in the mean. The Lagrangian integral time scale for  $\theta$  on  $\sigma_\theta = 26.60 \text{ kg m}^{-3}$ , computed for each float time series as detailed above, is  $40 (\pm 21)$  days. Assuming the array is sufficiently sparse spatially, about every four profiles should give 1 degree of freedom.

The regional seasonal cycle for  $\theta$  on  $\sigma_\theta = 26.60 \text{ kg m}^{-3}$  with 95% confidence limits (Fig. 6) shows that the isopycnal rapidly cools over the winter season, from a

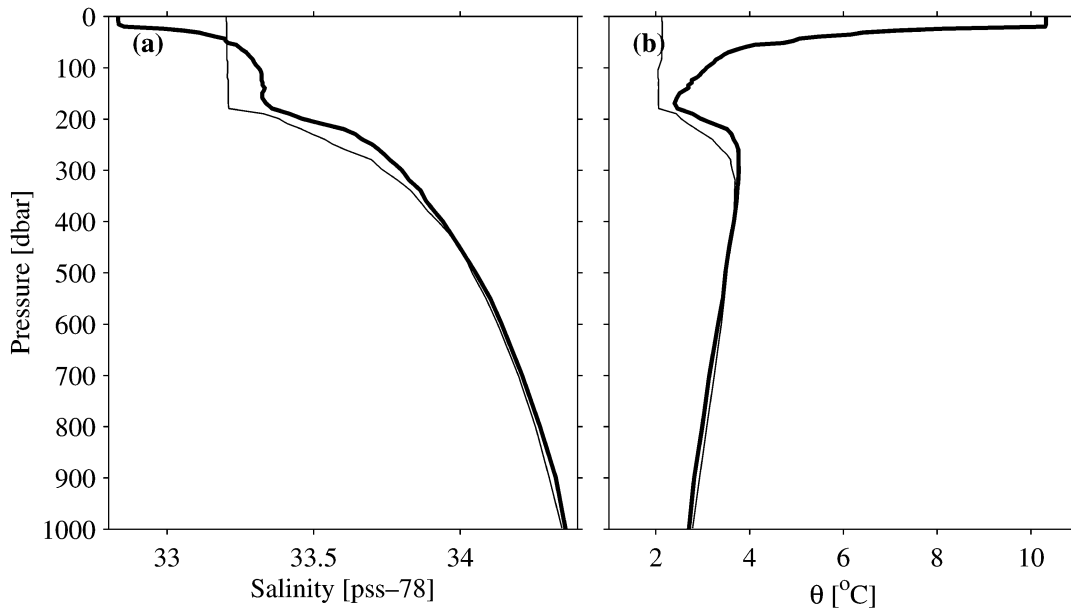


FIG. 5. Vertical profiles of (a) salinity and (b) potential temperature ( $\theta$ ) plotted against pressure. A summer profile taken at 56.56°N, 176.00°W on 21 Aug 2001 (thick lines) is contrasted with a winter profile taken at 56.77°N, 176.65°W on 16 Jan 2002 (thin lines).

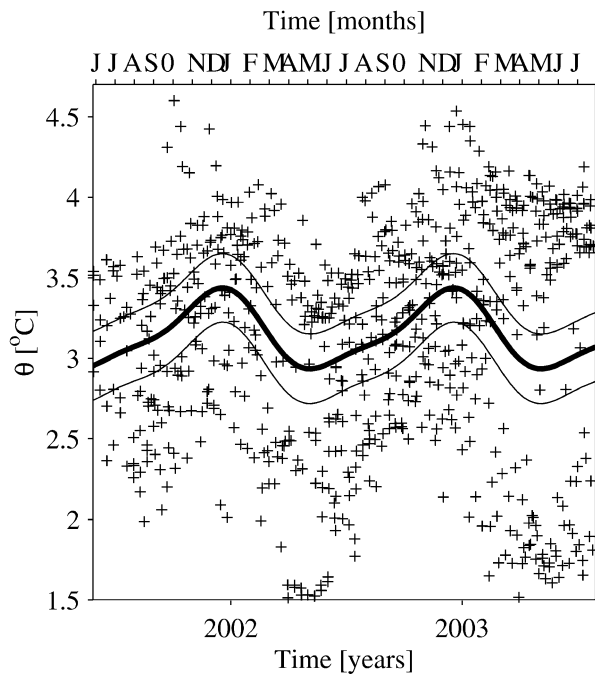


FIG. 6. Potential temperature ( $\theta$ ) on  $\sigma_\theta = 26.60 \text{ kg m}^{-3}$ , near the potential density of the shallow  $\theta$  minimum, from the Bering Sea float data (pluses) plotted against time. The seasonal cycle is described by fitting annual and semiannual harmonics to the data (thick line). The 95% confidence intervals for that fit (thin lines) assume the Lagrangian integral time scale of 40 days allows a degree of freedom for about every four data points.

high of 3.4°C in December to a low of 2.9°C in May. The rapid cooling is presumably because of the influence of winter surface cooling. This influence peaks in spring after the mixed layer is coldest, densest, and deepest, and  $\sigma_\theta = 26.60 \text{ kg m}^{-3}$  has been recently exposed to surface cooling, especially in the northwest portion of the array. Warming occurs more slowly over the rest of the year. This warming is presumably owing to some combination of mixing acting to reduce the temperature minimum, which is a vertical extrema, and advection of warmer Alaska Stream water into the Bering Sea through the southern island arc passes (Stabeno and Reed 2003, unpublished manuscript).

An objective map of  $\theta$  on  $\sigma_\theta = 26.60 \text{ kg m}^{-3}$ , with the seasonal cycle as fit above removed, shows a relatively clear spatial pattern, colder in the center of the basin and warmer near the boundaries (Fig. 7). The pattern is similar, although somewhat noisier, if the data are mapped without first removing the seasonal cycle (not shown), which is not surprising both since the seasonal cycle spans a relatively small portion of the overall range of the data (Fig. 6) and since removal of a regional seasonal cycle might help ameliorate deficiencies in spatiotemporal distribution of the array. The warm signature is strongest near its source, consisting of flow through and mixing within the island arc passes. These warm waters appear to be advected eastward along the southern boundary of the Aleutian Basin in the Aleutian North Slope Current and then northwestward along the northeastern boundary of the basin in the Bering Slope Current, as suggested by previous analyses discussed. The warm values around the edges are not continuous

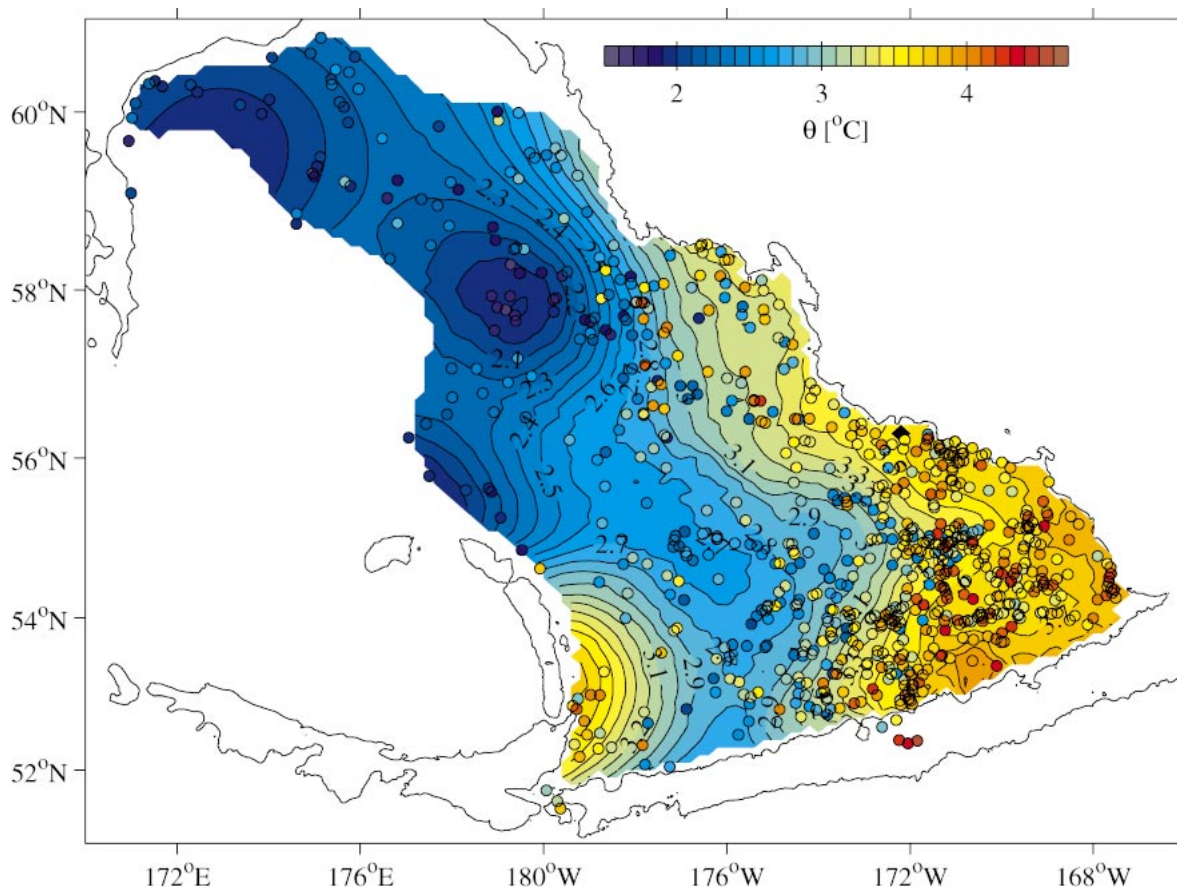


FIG. 7. Objective map of potential temperature ( $\theta$ ) on  $\sigma_\theta = 26.60 \text{ kg m}^{-3}$ , near the potential density of the shallow  $\theta$  minimum. A mean regional seasonal cycle (Fig. 6) is removed from the data prior to mapping. The map assumes a Gaussian covariance incorporating correlation scales of  $4^\circ$  lon,  $2^\circ$  lat, and  $2 \times 10^{-7} \text{ m}^{-1} \text{ s}^{-1}$  in potential vorticity (the Coriolis parameter  $f$  over water depth  $h$ ) and a noise-to-signal energy of 0.0625. Contours (at  $0.1^\circ\text{C}$  intervals) stop where mapping errors exceed the assumed noise-to-signal energy. Data values (dots) are shaded with the same color scale used for the contours.

at the southern boundary, which may well be due to temporal aliasing. As described above, the  $\theta$  field on  $\sigma_\theta = 26.60 \text{ kg m}^{-3}$  is subject to direct cooling by ventilation at the height of winter. Presumably the inflow of warmer waters from the Alaska Stream counterbalances the wintertime heat loss over the year.

For the entire float array in the Bering Sea, the mean and median potential densities of the subsurface  $\theta$  maximum are near  $26.82 \text{ kg m}^{-3}$ . On  $\sigma_\theta = 26.82 \text{ kg m}^{-3}$  the total range of  $\theta$  (not shown) is only  $0.7^\circ\text{C}$ , about a quarter of that on the lighter surface discussed above (Fig. 6). Any seasonal cycle is not significant at 95% confidence limits, but there is temporal variability of the  $\theta$  maximum itself in the southeastern Aleutian Basin, which is discussed below. The spatial pattern of  $\theta$  on  $\sigma_\theta = 26.82 \text{ kg m}^{-3}$  with or without this seasonal cycle removed is similar to that on the lighter surface discussed above, but much smaller in range. The pattern suggests that at this deeper level, too, warm salty water flows into the Bering Sea through the Aleutian passes and is advected cyclonically around the edges of the deep Bering Sea.

Temporal variability of the properties found at the subsurface temperature maximum in the southeast corner of the Aleutian Basin of the Bering Sea (south of  $55.5^\circ\text{N}$  and east of  $172^\circ\text{W}$ ) has been attributed to variability in the inflow to the Basin from the south through the Aleutian passes (Reed 1995a). Hydrographic surveys in some years show much warmer water associated with the Aleutian North Slope Current than in others. The means of water properties at the  $\theta$  maximum for the 182 profiles taken to date in that region ( $\theta \sim 3.85^\circ\text{C}$ ,  $\sigma_\theta \sim 26.76 \text{ kg m}^{-3}$ , and  $p \sim 286 \text{ dbar}$ ) are in the middle of regional historical values (Reed 1995a). Values of  $\theta$  at its subsurface maximum in this region (Fig. 8) do not approach the low end of previously reported ranges. Values also appear to be lower in the summer and higher in the winter. Although there are only about 26 months of data here, this pattern is consistent with a hypothesis that, when the gyre spins up in winter (Overland et al. 1994), more warm water from the south may be advected into the Bering Sea through the Aleutian passes (Stabeno and Reed 2003, unpublished manuscript). This connection of warm water advected through the passes

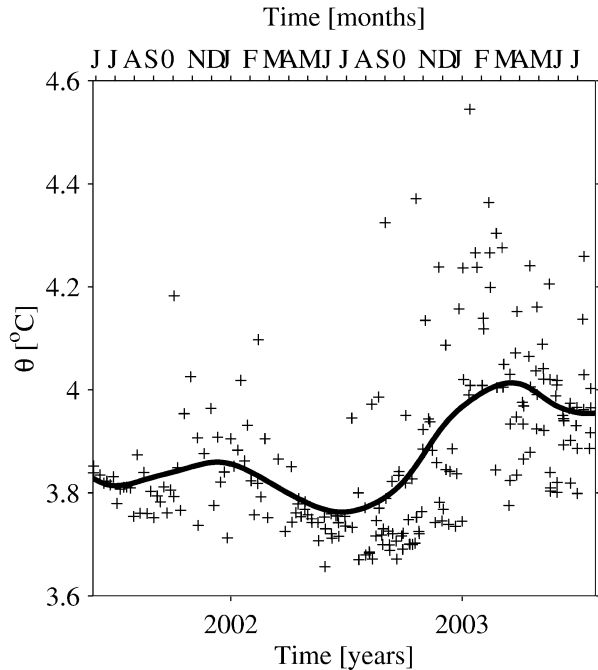


FIG. 8. Potential temperature ( $\theta$ ) at the subsurface  $\theta$  maximum from the float data (pluses) in southeastern (lat < 55.5°N, lon > 172°W) Aleutian Basin of the Bering Sea plotted against time. A smooth curve (thick line) is drawn using a loess filter with a 6-month half-power point (thick line).

and in the Bering Slope Current is supported on shorter time scales by satellite sea surface temperature analyses (Paluszkiwicz and Niebauer 1984). Last, values in the winter of 2002/03 are at the high end of the historical range, much higher than in the previous winter, consis-

tent with previous results showing significant interannual variability (Reed 1995a).

For a more detailed examination of the mean water property distributions associated with the Bering Slope Current, data from the same region used for the 1000-dbar float velocity estimates within the current (Fig. 1) are again analyzed as a function of range from the 1000-m isobath using data. The float  $\theta$  and  $S$  data are linearly interpolated to a 10-dbar pressure grid. Mean seasonal cycles (annual and semiannual harmonics) are fit to both water properties using all data within the region on each pressure surface. These seasonal cycles are removed. The data so modified are then smoothed as a function of range on each pressure surface using a loess filter (Cleveland and Devlin 1988) with a 60-km half power point. The spatial smoothing scale is appropriate to the current given cross-slope scales found from direct velocity analyses detailed above and geostrophic velocity analyses detailed below. This scale is also comparable to previously reported eddy scales in the region. However, including data over all times and along the entire length of the current helps to mitigate the effect of eddies on the mean. Of course, the procedure also averages over along-slope variations (e.g., the along-slope northwestward cooling in Fig. 7).

The resulting mean salinity section (Fig. 9a) illustrates several features associated with the Bering Slope Current. Of course,  $S$  increases monotonically downward as expected in the Bering Sea. The isohalines, which largely follow isopycnals (not shown), tilt downward as they approach the continental slope. This tilt is a signature of the along-slope geostrophic shear in this current, with surface-intensified northwestward flow.

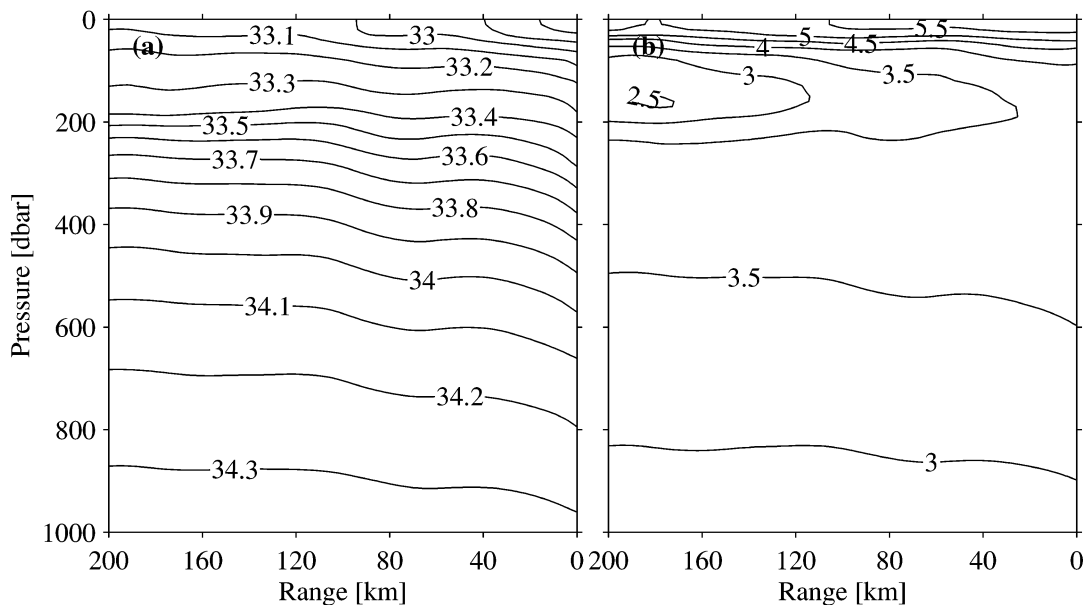


FIG. 9. Mean vertical sections of (a) salinity ( $S$ ) contoured at 0.1 intervals and (b) potential temperature ( $\theta$ ) contoured at 0.5°C intervals against pressure and range from the 1000-m isobath in the region of the Bering Slope Current.

There is clearly mean geostrophic shear associated with the current that extends all the way to 1000 dbar. Unfortunately, the infrequent sampling below 1000 dbar (every fourth profile extends to a target pressure of 2000 dbar) makes detailed analysis of water property distributions below 1000 dbar a dubious exercise at present. Another prominent feature is the significant freshening of surface water approaching the continental slope, a signature of the transition between open ocean and shelf waters (Kinder and Coachman 1978).

The mean  $\theta$  section (Fig. 9b) also reveals patterns typical of the Bering Slope Current. In the Bering Sea, salinity dominates the stratification, so temperature is closer to a passive tracer than in many other regions. The subsurface  $\theta$  minimum, found near 150 dbar, weakens toward the slope. This weakening is a signature of the Bering Slope Current and is caused by northward advection of warm water from the south within the current (Kinder et al. 1975). This pattern is also evident on isopycnal maps (Fig. 7). The more subtle subsurface  $\theta$  maximum is found between 300 and 400 dbar. It strengthens slightly (although not visibly) toward the slope, as expected given its southern source and the cyclonic circulation. The surface layer (roughly midway between summer and winter values, as expected since the seasonal cycle has been removed) has a  $\theta$  that increases slightly toward the continental slope.

## 5. Geostrophic flow

In addition to direct velocity estimates at the 1000-dbar park pressure, the floats allow application of the geostrophic relation over their sampling range to obtain circulation information. For three out of every four profiles, the floats have a target pressure of 1000 dbar for the deepest sample (every fourth profile targets 2000 dbar for its deepest sample). However, the floats sometimes take their deepest measurements slightly shallower than these target pressures. To retain these profiles, all geostrophic calculations are made relative to 990 dbar, which, given the weak vertical shears at this pressure, is not significantly different from the float 1000-dbar park pressure. There are many more profiles that reach 1900 dbar than reach 2000 dbar, so the deep calculations are made only to that lesser pressure. Since these calculations involve vertical integration, only profiles with data from all nominal pressures over the interval of interest are used, limiting the data set to 675 profiles between the surface and 990 dbar and 142 profiles reaching to 1900 dbar.

The transport function  $Q$  (Sverdrup et al. 1942, p. 463) is just the vertical integral of the geopotential anomaly, referenced as desired, between two pressures. This quantity is used here to analyze the geostrophic transport between the surface and 990 dbar and between 990 dbar and the deepest float pressures near 1900 dbar. The Lagrangian integral time scale for  $Q$  between the surface and 990 dbar relative to 990 dbar, computed as

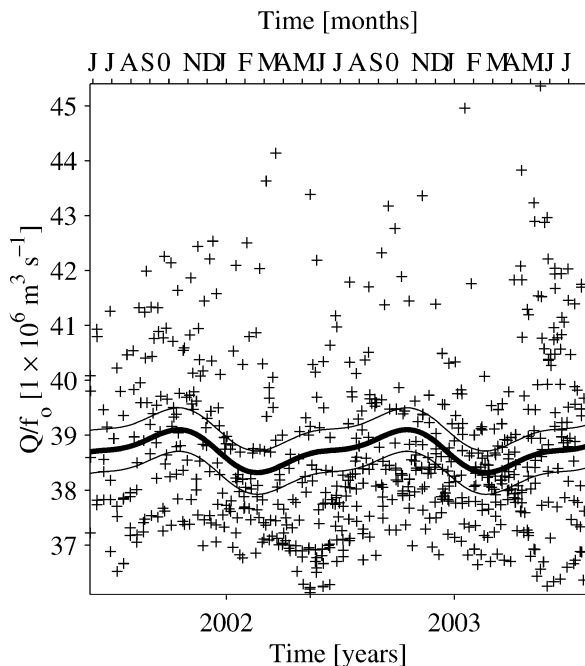


FIG. 10. Approximate transport streamfunction  $Q/f_o$  ( $1 \times 10^6 \text{ m}^3 \text{ s}^{-1}$ ) between the surface and 990 dbar, relative to 990 dbar, from the Bering Sea float data (pluses) plotted against time. A mean seasonal cycle is described by annual and semiannual harmonics fit to the data (thick line) with 95% confidence intervals for that fit (thin lines) assuming the Lagrangian integral time scale of 24 days for that quantity allows 2 degrees of freedom for about every five data points.

detailed above, is  $24 (\pm 13)$  days. Thus about every five  $Q$  estimates above 990 dbar give 2 degrees of freedom. Since  $Q$  estimates below 990 dbar can only be made every fourth cycle, they are assumed to be statistically independent.

Relative volume transports over these pressure ranges are locally parallel to  $Q$  isopleths. Transports between  $Q$  isopleths are found by dividing their difference by  $f$ , the local Coriolis parameter. If the range of the Coriolis parameter is small, an approximate relative transport stream function can be constructed from  $Q/f_o$ , where  $f_o = 1.26 \times 10^{-4} \text{ s}^{-1}$  is the Coriolis parameter for the central latitude of the region of interest,  $56.5^\circ \text{N}$  for the deep Bering Sea. This approximate transport streamfunction is negatively biased by about 5% at the southern limit of the deep Bering Sea and is positively biased by about 5% at its northern limit, small errors in comparison with other noise sources such as temporal variability. Differences of this quantity, not its absolute value, yield transport estimates, analogous to the relation between dynamic height gradients and geostrophic velocity.

The annual cycle of  $Q/f_o$  between the surface and 990 dbar relative to 990 dbar as described by annual and semiannual harmonics with 95% confidence intervals (Fig. 10) has its lowest values in February and highest values in October. When estimated over the entire basin the observed seasonal cycle reflects mostly

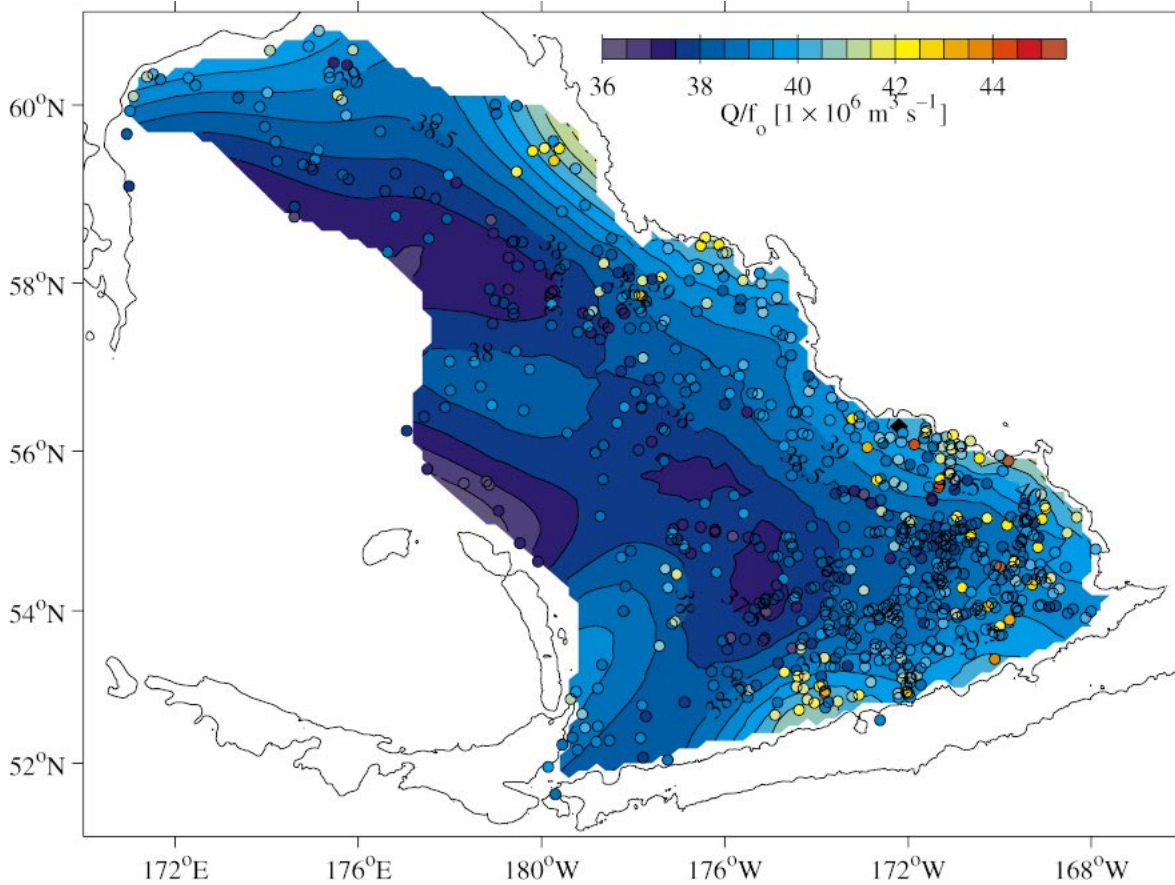


FIG. 11. Approximate transport streamfunction  $Q/f_0$  between the surface and 990 dbar, relative to 990 dbar, from the Bering Sea float data contoured at  $0.5 \times 10^6 \text{ m}^3 \text{ s}^{-1}$  intervals. Details follow Fig. 7.

the seasonal temperature variability from the upper ocean. This variability has no direct relation to seasonal transport variations within the basin since it does not involve a spatial difference in  $Q/f_0$ . The seasonal cycle is removed prior to further spatial analysis. Numerical model results suggest that there may also be a seasonal cycle in basin current transports (Overland et al. 1994) due to variability in wind forcing (Bond et al. 1994). However, this cycle cannot yet be estimated with the float data. There is no significant seasonal cycle in  $Q/f_0$  between 990 and 1900 dbar relative to 990 dbar (not shown), and so no harmonic fits are removed from that quantity. This lack of a seasonal cycle at depth is not surprising since seasonal heating and cooling in the deep ocean is very unlikely here.

An objective map of  $Q/f_0$  between the surface and 990 dbar relative to 990 dbar with the seasonal cycle removed reveals a familiar pattern, with relatively low values in the center of the basin and higher values around the periphery (Fig. 11). The higher values along the southern boundary of the Aleutian Basin are the signatures of the eastward flowing Aleutian North Slope Current. The higher values on the northeastern boundary of the Aleutian Basin are the signatures of the north-

westward flowing Bering Slope Current. The significant variability in the values, even after the mean seasonal cycle is removed, is primarily the signature of mesoscale eddies (Mizobata et al. 2002). The sampling density is not yet sufficient to overcome the effect of this variability as mapped. One might expect a relatively constant transport stream function around the rim of the Aleutian Basin. However, as a result of the influence of eddies, the mapped values at the boundary exceed the central minimum mapped value by between 1.0 and 4.5 Sv.

Analysis of  $Q/f_0$ , as a function of range from the 1000-m isobath within the Bering Slope Current region, allows estimates of current transport between the surface and 990 dbar relative to 990 dbar using 304 data points (Fig. 12a), and current transport between 990 and 1900 dbar relative to 990 dbar using 69 data points (Fig. 12b). The correlation coefficient of these quantities for profiles where both are estimated is  $-0.76$ , presumably due to general continuity in the sign of geostrophic shear across the reference level. Again, the seasonal cycle has been removed for the estimate above 990 dbar but not for that below. The 1900-dbar level is used here because it is the deepest level to which geostrophic transport

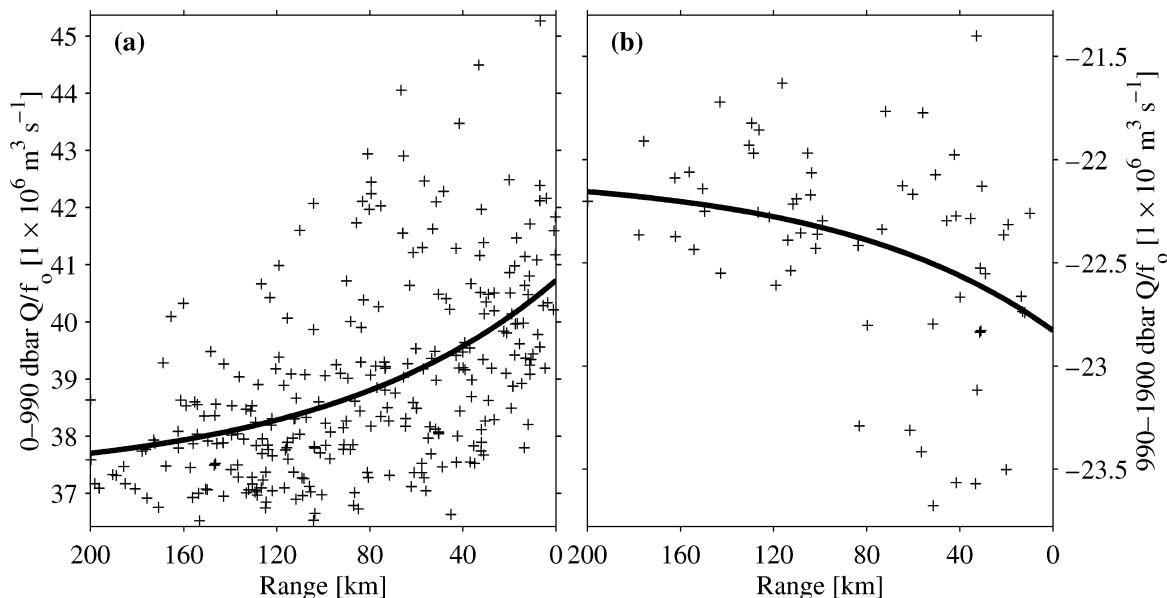


FIG. 12. Approximate transport streamfunctions  $Q/f_0$ , within the Bering Slope Current study region plotted against range from the 1000-m isobath for (a) between the surface and 990 dbar relative to 990 dbar, where the seasonal cycle is removed, and (b) between 990 and 1900 dbar relative to 990 dbar, where there is no seasonal cycle to remove. Exponential fits to  $Q/f_0$  vs range (thick lines) allow transport and lateral scale estimates for the current.

calculations can be made with most of the deep profiles. In addition, the combination of geostrophic and absolute transport between the surface and that level maximizes the along-slope current transport.

The geostrophic transport of the Bering Slope Current offshore of the 1000-m isobath depends on the difference of a value representative of  $Q/f_0$  at that isobath and some (constant, it is hoped) offshore value. Fitting an exponential function to these data versus range (Fig. 12) is one way to estimate the transport and lateral scale of the current. For the upper portion of the water column, this model gives a current transport of  $3.5 (\pm 1.1)$  Sv and a lateral scale of  $100 (\pm 97)$  km. The 95% uncertainties have been determined using a delete-one jackknife (Efron 1982), accounting for degrees of freedom. For the lower portion of the water column, the transport is estimated at  $-0.7 (\pm 0.4)$  Sv with a lateral scale of  $94 (\pm 103)$  km. The median distance between the 1000- and 1900-m isobaths is only 8 km between  $55^\circ$  and  $60^\circ$ N off the Bering Shelf. Thus, the lower portion of the transport is evaluated at 4 km offshore of the 1000-m isobath to take into account the reduction of transport owing to the bathymetry. The lateral scales agree well with each other, although their errors are large. They also agree well with scales from the direct current measurement analysis above. The deep transport value is negative (southeastward) only because it is computed relative to the approximate float park pressure of 990 dbar, a level at which analysis of the direct measurements above has revealed a significant positive (northwestward) flow within the Bering Slope Current.

## 6. Synthesis

Water property distributions, direct velocity measurements at the 1000-dbar float park pressure, and geostrophic transport estimates relative to near that park pressure all reveal robust signatures of the Bering Slope Current. The mean along-slope velocity estimates made at 1000 dbar from direct measurements within the current region yield an along-slope transport of  $3.0 (\pm 0.9)$  Sv (Fig. 4b) when applied uniformly in the vertical to the upper 1900 dbar from the 1000-m isobath to 120 km offshore of that isobath. This value can be combined with the geostrophic transport estimates relative to 990 dbar, between the surface and 990 dbar and between 990 and 1900 dbar (Fig. 12). The result is an absolute geostrophic estimate of the current transport,  $5.8 (\pm 1.7)$  Sv above 1900 dbar and offshore of the 1000-m isobath. The large correlation between  $Q/f_0$  above and below 990 dbar has been taken into account in propagating errors for the 95% confidence interval quoted, as have the number of degrees of freedom for each component of the transport estimate. The float park pressure velocity estimates contribute nearly one-half of the total transport of the current when applied over this pressure interval and integrated.

As mentioned previously, the pressure interval of 0–1900 dbar has been chosen mainly because most of the floats do not sample deeper than 1900 dbar. This choice also maximizes the Bering Slope Current transport when relative geostrophic estimates are combined with direct velocity estimates at the reference level. Nevertheless, the absolute geostrophic transport over the pressure in-

terval of 0–990 dbar is  $5.1 (\pm 1.2)$  Sv, not much more than that for 0–1900 dbar. The rate of increase in absolute geostrophic transport estimates for integrations to increasingly higher pressures tapers off slowly. These results suggest that the current signature, while falling off with depth, extends well below 1000 dbar, reaching at least 1900 dbar, consistent with previous full-depth studies of currents in the region (Roden 1995; Cokelet et al. 1996).

The floats also do not sample inshore of the 1000-m isobath, and so the Bering Slope Current estimate presented here is limited to the flow offshore of the 1000-m isobath. The flow inshore of the shelf break near the 170-m isobath is relatively weak (order  $0.01\text{--}0.1\text{ m s}^{-1}$ ) and is not classified as part of the Bering Slope Current (Schumacher and Kinder 1983). The flow between the shelf break and the 1000-m isobath may be stronger (Kinder et al. 1975) but is difficult to quantify because the continental slope is so steep there. The median distance between the 1000-m isobath and the 170-m depth shelf break is only 11 km off the Bering Shelf between  $55^\circ$  and  $60^\circ\text{N}$ . This short distance makes geostrophic calculations from synoptic surveys subject to aliasing by high-frequency energy such as internal tides. Extrapolation of the exponential model of  $Q/f_o$  for the upper portion of the water column (Fig. 12a) to 11 km inshore of the 1000-m isobath suggests that something near  $0.4\text{ Sv}$  is an upper bound to the missed transport. The actual missed transport is likely to be even smaller because of the shoaling between the 1000-m isobath and the shelf break.

*Acknowledgments.* This work was funded by the NOAA National Marine Fisheries Service Steller Sea Lion Coordinated Research Program and the NOAA Office of Oceanic and Atmospheric Research. The work would not have been possible without the very able assistance of Dana Swift and Dale Ripley in float preparation, Donald Denbo and Kristene McTaggart in float data management, and many helpful colleagues in float deployment. Constructive comments from two anonymous reviewers and useful conversations with Ron Reed also contributed to improving the manuscript.

#### REFERENCES

- Bond, N. A., J. E. Overland, and P. Turet, 1994: Spatial and temporal characteristics of the wind forcing of the Bering Sea. *J. Climate*, **7**, 1119–1130.
- Chelton, D. B., R. A. deSzoeke, M. G. Schlax, K. El Naggar, and N. Siwertz, 1998: Geographical variability of the first baroclinic Rossby radius of deformation. *J. Phys. Oceanogr.*, **28**, 433–460.
- Cleveland, W. S., and S. J. Devlin, 1988: Locally weighted regression: An approach to regression analysis by local fitting. *J. Amer. Stat. Assoc.*, **83**, 596–610.
- Cokelet, E. D., and P. J. Stabeno, 1997: Mooring observations of the thermal structure, salinity, and currents in the SE Bering Sea basin. *J. Geophys. Res.*, **102**, 22 947–22 964.
- , M. L. Schall, and D. M. Dougherty, 1996: ADCP-referenced geostrophic circulation in the Bering Sea Basin. *J. Phys. Oceanogr.*, **26**, 1113–1128.
- Davis, R. E., 1998: Preliminary results from directly measuring mid-depth circulation in the tropical and South Pacific. *J. Geophys. Res.*, **103**, 24 619–24 639.
- , D. C. Webb, L. A. Regier, and J. Dufour, 1992: The Autonomous Lagrangian Circulation Explorer (ALACE). *J. Atmos. Oceanic Technol.*, **9**, 264–285.
- Efron, B., 1982: *The Jackknife, the Bootstrap, and Other Resampling Plans*. CBMS-NSF Regional Conference Series in Applied Mathematics, Vol. 38, SIAM, 92 pp.
- Emery, W. J., and R. E. Thompson, 1997: *Data Analysis Methods in Physical Oceanography*. Elsevier Science, 634 pp.
- Kinder, T. H., and L. K. Coachman, 1978: The front overlaying the continental slope in the eastern Bering Sea. *J. Geophys. Res.*, **83**, 4551–4559.
- , —, and J. A. Galt, 1975: The Bering Slope Current System. *J. Phys. Oceanogr.*, **5**, 231–244.
- , J. D. Schumacher, and D. V. Hansen, 1980: Observation of a baroclinic eddy: An example of mesoscale variability in the Bering Sea. *J. Phys. Oceanogr.*, **10**, 1228–1245.
- Miura, T., T. Suga, and K. Hanawa, 2003: Numerical study of formation of dichothermal water in the Bering Sea. *J. Oceanogr.*, **59**, 369–376.
- Mizobata, K., and Coauthors, 2002: Bering Sea cyclonic and anticyclonic eddies observed during summer 2000 and 2001. *Progress in Oceanography*, Vol. 55, Pergamon, 65–75.
- Okkonen, S. R., 2001: Altimeter observations of the Bering Slope Current eddy field. *J. Geophys. Res.*, **106**, 2465–2476.
- Overland, J. E., M. C. Spillane, H. E. Hurlburt, and A. J. Wallcraft, 1994: A numerical study of the Bering Sea Basin and exchange with the North Pacific Ocean. *J. Phys. Oceanogr.*, **24**, 736–758.
- Paluszkiwicz, T., and H. J. Niebauer, 1984: Satellite observations of circulation in the eastern Bering Sea. *J. Geophys. Res.*, **89**, 3663–3678.
- Poulain, P.-M., and P. P. Niiler, 1989: Statistical analysis of the surface circulation in the California Current system using satellite-tracked drifters. *J. Phys. Oceanogr.*, **19**, 1588–1603.
- Reed, R. K., 1995a: On the variable subsurface environment of fish stocks in the Bering Sea. *Fish. Oceanogr.*, **4**, 317–323.
- , 1995b: On geostrophic reference levels in the Bering Sea. *J. Oceanogr.*, **51**, 489–498.
- , and P. J. Stabeno, 1994: Flow along and across the Aleutian Ridge. *J. Mar. Res.*, **52**, 639–648.
- Roden, G. I., 1995: Aleutian Basin of the Bering Sea: Thermohaline, oxygen, nutrient and current structure in July 1993. *J. Geophys. Res.*, **100**, 13 539–13 554.
- Sayles, M. A., K. Aagaard, and L. K. Coachman, 1979: *Oceanographic Atlas of the Bering Sea Basin*. University of Washington Press, 158 pp.
- Schumacher, J. D., and T. H. Kinder, 1983: Low-frequency current regimes over the Bering Sea shelf. *J. Phys. Oceanogr.*, **13**, 607–623.
- , and R. K. Reed, 1992: Characteristics of currents over the continental slope of the eastern Bering Sea. *J. Geophys. Res.*, **97**, 9423–9433.
- , and P. J. Stabeno, 1994: Ubiquitous eddies of the eastern Bering Sea and their coincidence with concentrations of larval pollack. *Fish. Oceanogr.*, **3**, 182–190.
- Smith, W. H. F., and D. T. Sandwell, 1997: Global sea floor topography from satellite altimetry and ship depth soundings. *Science*, **277**, 1956–1962.
- Stabeno, P. J., and R. K. Reed, 1992: A major circulation anomaly in the western Bering Sea. *Geophys. Res. Lett.*, **19**, 1671–1674.
- , and —, 1994: Circulation in the Bering Sea Basin observed by satellite-tracked drifters: 1986–1993. *J. Phys. Oceanogr.*, **24**, 848–854.
- , J. D. Schumacher, and K. Ohtani, 1999: The physical oceanography of the Bering Sea. *Dynamics of the Bering Sea: A Summary of Physical, Chemical, and Biological Characteristics, and*

- a Synopsis of Research on the Bering Sea*, T. R. Loughlin and K. Ohtani, Eds., North Pacific Marine Science Organization (PICES) and University of Alaska Sea Grant, AK-SG-99-03, 1–28.
- Sverdup, H. U., M. W. Johnson, and R. H. Fleming, 1942: *The Oceans: Their Physics, Chemistry, and General Biology*. Prentice Hall, 1087 pp.
- Verkhunov, A. V., and Y. Y. Tkachenko, 1992: Recent observations of variability in the western Bering Sea current system. *J. Geophys. Res.*, **97**, 14 369–14 376.
- Wong, A. P. S., G. C. Johnson, and W. B. Owens, 2003: Delayed-mode calibration of autonomous CTD profiling float salinity data by theta-S climatology. *J. Atmos. Oceanic Technol.*, **20**, 308–318.